

Dynamic analysis of wind-vehicle-bridge systems using mutually-affected aerodynamic parameters

Bin Wang^{*1,2,3}, You-Lin Xu^{**2} and Yongle Li^{1,3a}

¹Department of Bridge Engineering, Southwest Jiaotong University, Chengdu, China

²Department of Civil and Environmental Engineering, The Hong Kong Polytechnic University, Hong Kong, China

³Key Laboratory of High-speed Railway Engineering (Southwest Jiaotong University), Ministry of Education, Chengdu, Sichuan 610031, China

(Received November 9, 2014, Revised December 29, 2014, Accepted January 5, 2015)

Abstract. Several frameworks for the dynamic analysis of wind-vehicle-bridge systems were presented in the past decade to study the safety or ride comfort of road vehicles as they pass through bridges under crosswinds. The wind loads on the vehicles were generally formed based on the aerodynamic parameters of the stationary vehicles on the ground, and the wind loads for the pure bridge decks without the effects of road vehicles. And very few studies were carried out to explore the dynamic effects of the aerodynamic interference between road vehicles and bridge decks, particularly for the moving road vehicles. In this study, the aerodynamic parameters for both the moving road vehicle and the deck considering the mutually-affected aerodynamic effects are formulized firstly. And the corresponding wind loads on the road vehicle-bridge system are obtained. Then a refined analytical framework of the WVB system incorporating the resultant wind loads, a driver model, and the road roughness in plane to fully consider the lateral motion of the road vehicle under crosswinds is proposed. It is shown that obvious lateral and yaw motions of the road vehicle occur. For the selected single road vehicle passing a long span bridge, slight effects are caused by the aerodynamic interference between the moving vehicle and deck on the dynamic responses of the system.

Keywords: wind-vehicle-bridge system; aerodynamic parameter; interference; moving vehicle

1. Introduction

To meet the requirements of modern society for convenient transportation systems, many long span bridges have been built around the world. The probability becomes higher and higher that road vehicles running on bridges are subject to crosswinds. Since long span bridges tend to be flexible and lightly damped, considerable wind-induced vibrations happen within a wide range of wind speeds. As road vehicles moves on the long span bridges under crosswind, the dynamic responses and aerodynamic characteristics of the vehicles and bridges are affected mutually with

*Corresponding author, Ph.D., E-mail: wangbinwvb@swjtu.edu.cn

**Co-corresponding author, Chair Professor, E-mail: ceylxu@polyu.edu.hk

^a Professor, Email: lele@swjtu.edu.cn

each other. Several frameworks for the dynamic analysis of wind-vehicle-bridge systems (WVB) were presented. Xu and Guo (2003) constructed a coupled WVB system using a fully computerized approach. In this system, vehicles were modeled as mass-spring-damper systems while bridges were modeled by the Finite Element Method (FEM). Random crosswinds were simulated and the corresponding wind forces were applied to both vehicles and bridges. Road roughness was also simulated in random and attached on the surface of the bridge deck. Cai and Chen (2004) presented a framework for the dynamic analysis of the WVB system. The simulated vehicle responses including the vertical, rolling, and pitching responses, and the lateral acceleration of the bridge were then input to a separated vehicle model to find the lateral responses of the vehicle (Chen and Cai 2004). Cheung and Chan (2010) considered three aspects for the coupled WVB system: the wind-bridge interaction, the wind-vehicle interaction, and the vehicle-bridge interaction. Han *et al.* (2014) tested the aerodynamic parameters for the status of stationary road vehicles distributed on a bridge deck and analyzed the responses of the vehicles and the bridge. In the WVB systems for rail vehicles, some models have also been developed, such as in Xu *et al.* (2003), Kwon *et al.* (2008), Xia *et al.* (2008), Chen *et al.* (2011). The aerodynamic parameters did not consider the aerodynamic interference between the rail vehicles and the bridges. In the WVB model of Li *et al.* (2005), the aerodynamic parameters for a stationary train-bridge system were tested to consider the aerodynamic interference.

In the above frameworks of the WVB systems, wind loads acting on vehicles were formed mainly based on the aerodynamic parameters of stationary vehicles on the ground. The wind loads acting on the bridge decks were also mainly generated without considering the influences of the vehicles. Although the aerodynamic interference were considered in Li *et al.* (2005) for a train and Han *et al.* (2014) for road vehicles, the effects of moving road vehicle have not been put forward. As vehicles move on the bridge deck and the flows around the pure deck are altered naturally by the passing of the vehicles, the aerodynamic forces on the bridge deck are, therefore, changed by the movement of the vehicles (Wang *et al.* 2013). In this study, the aerodynamic parameters for both the vehicle and deck considering the mutually-affected aerodynamic effects are formulized firstly. The corresponding wind loads on the road vehicle-bridge system are then obtained. The refined analytical framework of WVB incorporating a driver, road roughness in plane (considering the roughness difference in both the moving and lateral direction) is proposed to fully consider the lateral motion of the road vehicle under crosswind.

2. Wind loads on a road vehicle

Wind loads on a moving vehicle have been derived based on the quasi-steady assumption in Wang (2014) considering the timely attitude of the vehicle and rewritten as

$$f_{vy}^W = \frac{1}{2} \rho U_{re}^2 A_f [C_S(\alpha_w) + C'_S(\alpha_w) \beta_w] \quad (1a)$$

$$f_{vz}^W = \frac{1}{2} \rho U_{re}^2 A_f [C_L(\alpha_w) + C'_L(\alpha_w) \beta_w] \quad (1b)$$

$$m_{vx}^W = \frac{1}{2} \rho U_{re}^2 A_f L_v [C_R(\alpha_w) + C'_R(\alpha_w) \beta_w] \tag{1c}$$

$$m_{vy}^W = \frac{1}{2} \rho U_{re}^2 A_f L_v [C_P(\alpha_w) + C'_P(\alpha_w) \beta_w] \tag{1d}$$

$$m_{vz}^W = \frac{1}{2} \rho U_{re}^2 A_f L_v [C_Y(\alpha_w) + C'_Y(\alpha_w) \beta_w] \tag{1e}$$

with

$$U_{re} = \sqrt{U_{xe}^2 + U_{ye}^2 + U_{ze}^2} \tag{2a}$$

$$\alpha_w = \arctan\left(\frac{\sqrt{U_{ye}^2 + U_{ze}^2}}{U_{xe}}\right) \tag{2b}$$

$$\beta_w = \arctan\left(\frac{U_{ze}}{U_{ye}}\right) \tag{2c}$$

where the subscripts x , y , and z are the three orthogonal coordinate axes attached on the vehicle body; f_{vy}^W and f_{vz}^W are the wind forces along the y - and z -axis, respectively; m_{vx}^W , m_{vy}^W , and f_{vz}^W are the wind induced moments around the x -, y -, and z -axis, respectively; ρ is the density of air; A_f is a reference area; L_v is the length of the vehicle; U_{xe} , U_{ye} , and U_{ze} represent the relative wind components to the vehicle along the x -, y -, and z -axis, respectively; C_S , C_L , C_P , C_Y , and C_R are the corresponding aerodynamic coefficients. The aerodynamic coefficients of a moving vehicle on a bridge deck at different relative yaw angles (α_w) have been computed in Wang *et al.* (2013). 3-order polynomials can be fitted for those aerodynamic coefficients as

$$C_i(\alpha_w) = C_{i0} + C_{i1}\alpha_w + C_{i2}\alpha_w^2 + C_{i3}\alpha_w^3 \tag{3}$$

where C_{ij} ($i=S, L, P, Y, R$ and $j=0, 1, 2, 3$) are the fitting constants.

3. Wind loads on a bridge

As a road vehicle moves on a long span bridge, the wind loads acting on the bridge deck are more dominant to affect the ride of the vehicle compared with the wind loads on other parts of the bridge such as towers. Therefore, wind loads acting on only the deck of the bridge were considered in the framework of the WVB system as in Xu and Guo (2003), Cai and Chen (2004), and Cheung and Chan (2010). This approximation is also taken in this study and wind loads on only the bridge deck are applied. The wind loads on a bridge deck are usually decomposed according to the nature of wind induced forces as three components: static wind loads, buffeting loads and self-excited loads

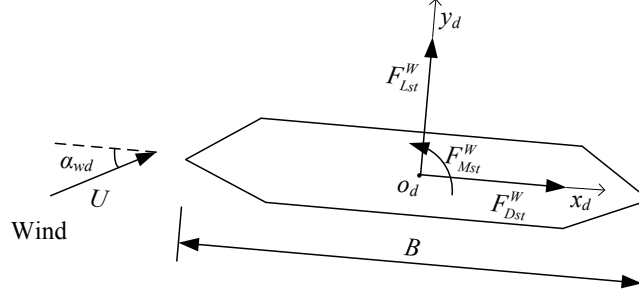


Fig. 1 Static wind loads on the cross section of deck

$$\mathbf{F}_b^W = \mathbf{F}_{bst}^W + \mathbf{F}_{bfl}^W + \mathbf{F}_{bse}^W \quad (4)$$

where \mathbf{F}_b^W is the wind load vector; \mathbf{F}_{bst}^W , \mathbf{F}_{bfl}^W , and \mathbf{F}_{bse}^W represent the vectors of the static wind loads, buffeting loads, and self-excited loads acting on the nodes of the bridge deck, respectively. In this study, the wind loads on each node are integrated from the wind loads on the section of deck along half length/lengths of the element/elements possessing the node.

3.1 Static wind loads

Static wind loads are the forces due to the mean winds. Fig. 1 illustrates the cross section on a pure deck (pure deck in this study means deck without vehicles on it). A local coordinate system $x_d O_d y_d$ is attached with the origin on the centroid, with the x_d -axis and y_d -axis along the horizontal and vertical directions of the cross section. The static wind loads on the cross section are composed of the drag force F_{Dst}^W along the x_d -axis, lift force F_{Lst}^W along the y_d -axis and the moment F_{Mst}^W around O_d . In the previous WVB analyses (Xu and Guo 2003, Cai and Chen 2004, Cheung and Chan 2010), the aerodynamic coefficients of a pure deck without taking into account the effects of the moving road vehicle were adopted since there are no tested or computed results for the actual moving vehicle on the bridge. In Wang *et al.* (2013), the aerodynamic coefficients of a bridge deck under a moving road vehicle are computed. They vary with not only the locations of the vehicle d_v on the deck, but also the relative angle between the velocity of the vehicle and the winds α_{wv} . The wind loads acting on the deck have to be expressed to include the effects of the moving vehicle as follows

$$F_{Dst}^W = \frac{1}{2} \rho U^2 C_{DV} (\alpha_{wd}, \alpha_{wv}, d_v) B \quad (5a)$$

$$F_{Lst}^W = \frac{1}{2} \rho U^2 C_{LV} (\alpha_{wd}, \alpha_{wv}, d_v) B \quad (5b)$$

$$F_{Mst}^W = \frac{1}{2} \rho U^2 C_{MV} (\alpha_{wd}, \alpha_{wv}, d_v) B^2 \quad (5c)$$

where ρ is the air density; U is the mean wind velocity; B is the width of the deck; C_{DV} , C_{LV} , and C_{MV} are the static aerodynamic coefficients of the drag, lift, and moment on the deck, considering the effects of the moving vehicle on the bridge deck, respectively; α_{wd} is the angle of attack. It is assumed that the effects of the moving vehicle on the static aerodynamic coefficients of the deck alter very slightly with the attack angle of wind. The static aerodynamic coefficient C_{iV} can thus be approximated as

$$C_{iv}(\alpha_{wd}, \alpha_{wv}, d_v) \approx C_i(\alpha_{wd}) R_i(\alpha_{wv}, d_v) \quad i=D, L, M \quad (6)$$

where C_i is the static aerodynamic coefficient of the pure deck; R_i can be denoted as the aerodynamic influence factor of the moving vehicle on the static aerodynamic coefficients of the deck and it is the function of d_v and α_{wv} . It is very difficult to draw an explicit expression for R_i directly. A simple and useful way is used to identify the influence factor R_i through a process of Standardization and Segmental Averaging (SSA for short). This procedure involves the following three steps.

(1) Dividing segments

The aerodynamic coefficients of the bridge deck under and near the vehicle actually vary with location. The deck under the vehicle is, therefore, divided into several segments. Three equal segments are set for the deck right under the vehicle. The length of each segment is $L_v/3$ (with L_v is the length of the vehicle). Since the influenced range of the vehicle on the aerodynamic coefficients of the deck is mainly within a length about 7 times the length of the vehicle (Wang *et al.* 2013), thus, totally 21 segments are set for the deck influenced by the vehicle. The segments are numbered with $j=-10, -9...9, 10$ from left to right and $j=-1, 0$ and 1 are the position of the vehicle.

(2) Averaging aerodynamic coefficients

The averaged aerodynamic coefficient of the j th segment C_{ivj} is to represent the coefficient of the entire segment, and it can be obtained by averaging

$$C_{ivj} = \frac{3}{L_v} \int_j C_{iv} dz \quad (7)$$

(3) Standardization

The aerodynamic coefficient C_i of the bridge deck being not influenced by the vehicle can be taken as the average value of the aerodynamic coefficients of the two end segments as

$$C_i = \frac{1}{2} (C_{ivj}|_{j=-10} + C_{ivj}|_{j=10}) \quad (8)$$

The influence factor R_i of the j th segment can thus be calculated as

$$R_{ij} = \frac{C_{ivj}}{C_i} \quad (9)$$

Through the process of SSA, the aerodynamic coefficients of the bridge deck varying with the location of the vehicle can be obtained for each relative yaw angle α_{wv} . For each segment, the influence factor R_i is fitted with α_{wv} based on the results at different α_{wv} in Wang *et al.* (2013) using the 2-order polynomials as follows

$$R_{ij}(\alpha_{wv}) = C_{ij0} + C_{ij1}\alpha_{wv} + C_{ij2}\alpha_{wv}^2 \quad (10)$$

where C_{ij0} , C_{ij1} , and C_{ij2} are the fitting constants.

3.2 Buffeting loads

Buffeting loads are the forces induced by the fluctuations of incoming winds. Corresponding to the three directions of the local coordinate system of the deck, the buffeting loads are decomposed as the buffeting drag force F_{Dbl}^W along the x_d -direction, buffeting lift force F_{Lst}^W along the y_d -direction, and the moment F_{Mst}^W around the origin o_d . Based on the quasi-steady theory, they are expressed by Scanlan (1978). If considering the aerodynamic coefficients of the deck under moving vehicles, the static aerodynamic coefficients shall be replaced by $C_i(\alpha_{wd}) R_i(\alpha_{wv}, d_v)$ as in Eq. (6). And the derivative of C_{iV} respect to α_{wd} is approximated with $C'_i(\alpha_{wd})R_i(\alpha_{wv}, d_v)$. As a result, the fluctuating loads are updated as follows

$$F_{Dbl}^W(t) = \frac{1}{2} \rho U^2 B R_i(\alpha_{wv}, d_v) \left[2C_D(\alpha_{wd}) \chi_{Du} \frac{u(t)}{U} + C'_D(\alpha_{wd}) \chi_{Dw} \frac{w(t)}{U} \right] \quad (11a)$$

$$F_{Lbl}^W(t) = \frac{1}{2} \rho U^2 B R_i(\alpha_{wv}, d_v) \left[2C_L(\alpha_{wd}) \chi_{Lu} \frac{u(t)}{U} + (C'_L(\alpha_{wd}) + C_D(\alpha_{wd})) \chi_{Lw} \frac{w(t)}{U} \right] \quad (11b)$$

$$F_{Mbl}^W(t) = \frac{1}{2} \rho U^2 B^2 R_i(\alpha_{wv}, d_v) \left[2C_M(\alpha_{wd}) \chi_{Mu} \frac{u(t)}{U} + C'_M(\alpha_{wd}) \chi_{Mw} \frac{w(t)}{U} \right] \quad (11c)$$

where $C'_i(\alpha_{wd})$ ($i=D, L, \text{ and } M$) is the slope of $C_i(\alpha_{wd})$; $u(t)$ and $w(t)$ are the fluctuating wind speeds along, and perpendicular to, the mean wind direction; χ_{Lu} , χ_{Lw} , χ_{Pu} , χ_{Mu} , χ_{Mw} are the aerodynamic admittance functions.

3.3 Self-excited loads

Self-excited loads are the forces induced by the movement of the deck. Similar to the static and fluctuating wind loads, the self-excited loads on the cross section of a pure deck can be decomposed as three components: self-excited drag force F_{Dse}^W along the x_d -direction, self-excited lift force F_{Lse}^W along the y_d -direction, and self-excited moment F_{Mse}^W around the origin o_d . They can be expressed in the form of convolution integrals (Bucher and Lin, 1988) as follows:

$$F_{Dse}^W(t) = \int_{-\infty}^t f_{Dh}(t-\tau)h(\tau)d\tau + \int_{-\infty}^t f_{Dp}(t-\tau)p(\tau)d\tau + \int_{-\infty}^t f_{D\alpha}(t-\tau)\alpha(\tau)d\tau \quad (12a)$$

$$F_{Lse}^W(t) = \int_{-\infty}^t f_{Lh}(t-\tau)h(\tau)d\tau + \int_{-\infty}^t f_{Lp}(t-\tau)p(\tau)d\tau + \int_{-\infty}^t f_{L\alpha}(t-\tau)\alpha(\tau)d\tau \quad (12b)$$

$$F_{Mse}^W(t) = \int_{-\infty}^t f_{Mh}(t-\tau)h(\tau)d\tau + \int_{-\infty}^t f_{Mp}(t-\tau)p(\tau)d\tau + \int_{-\infty}^t f_{M\alpha}(t-\tau)\alpha(\tau)d\tau \quad (12c)$$

where $h(\tau)$, $p(\tau)$, and $\alpha(\tau)$ are the vertical, lateral, and rotational displacements of the bridge deck at time τ ; f_{ik} ($i = D, L, M$; $k = p, h, \alpha$) are the response functions of unit impulse displacement of k and can be calculated from the flutter derivatives of the pure deck. As the vehicles move on the bridge in normal condition, the wind speed is much smaller than the critical wind velocity of the bridge. As a result, the resulted bridge responses are not large. Therefore, the self-excited loads on the bridge deck are also limited. In this regard, the effects of the moving vehicle on the flutter derivatives are neglected.

4. Analytical framework of WVB

In the proposed framework of WVB system, the moving road vehicle and the long span bridge are treated as two subsystems under crosswinds. They are coupled together through the contact forces and the geometric compatibility between the vehicle wheels and the surface of the bridge deck.

4.1 Vehicle subsystem

The vehicle model is represented using a lumped mass vehicle model with a series of springs and dashpots, and the equation of motion is established on the local coordinate system of the vehicle body (VCS). The vehicle can move laterally, and the wheels can lose contact with the road surface in a physically rational way under the effects of crosswinds, drivers, and the road roughness in plane. The equations of motion of the road vehicle in the local coordinates of the vehicle body have been derived in Wang (2014) and rearranged as

$$m_{vb}\dot{v}_{vby} + m_{vb}\omega_{vbx}v_{vbx} - m_{vb}\omega_{vbx}v_{vbx} = f_{vby}^S - f_{vby}^G + f_{vy}^W \quad (13a)$$

$$m_{vb}\dot{v}_{vbx} - m_{vb}\omega_{vby}v_{vbx} + m_{vb}\omega_{vbx}v_{vby} = f_{vbx}^S - f_{vbx}^G + f_{vx}^W \quad (13b)$$

$$I_{xx}\dot{\omega}_{vbx} - I_{xz}\dot{\omega}_{vbx} + (I_{zz} - I_{yy})\omega_{vby}\omega_{vbx} - I_{xz}\omega_{vbx}\omega_{vby} = m_{vbx}^S + m_{vx}^W \quad (13c)$$

$$I_{yy}\dot{\omega}_{vby} + (I_{xx} - I_{zz})\omega_{vbx}\omega_{vbx} - I_{xz}(\omega_{vbx}^2 - \omega_{vby}^2) = m_{vby}^S + m_{vy}^W \quad (13d)$$

$$I_{zz}\dot{\omega}_{vbx} - I_{zx}\dot{\omega}_{vbx} + (I_{yy} - I_{xx})\omega_{vbx}\omega_{vby} + I_{xz}\omega_{vby}\omega_{vbx} = m_{vbx}^S + m_{vx}^W \quad (13e)$$

$$m_{wi}\dot{v}_{wiy} = f_{wiy}^S + f_{wiy}^G + f_{wiy}^T \quad (13f)$$

$$m_{wi}\dot{v}_{wiz} = f_{wiz}^S + f_{wiz}^G + f_{wiz}^T \quad (13g)$$

where the subscript v , vb , and wi represent the vehicle, vehicle body and the i th wheel, respectively; the subscript x , y , and z are the three orthogonal directions of the VCS; the superscript S , G , and W represent the suspension system, gravity, and wind, respectively; m_{vb} and m_{wi} is the mass of the vehicle body and the i th wheel, respectively; I_{xx} , I_{yy} , and I_{zz} are the moments of inertia of the vehicle body around the x -axis, y -axis, and z -axis, respectively; I_{xz} is the product of inertial of the

vehicle body in the xz plane; v_{vby} and v_{vzb} are the transitional velocities of the vehicle body along the y -axis and z -axis, respectively; ω_{vbx} , ω_{vby} , and ω_{vzb} are the angular velocities of the vehicle body around the x -axis, y -axis, and z -axis, respectively; v_{wiy} and v_{wiz} are the transitional velocities of the i th wheel along the y -axis and z -axis, respectively; f_{vby}^G and f_{vzb}^G are the gravity components of the vehicle body along the y -axis and z -axis, respectively; f_{wiy}^G and f_{wiz}^G are the gravity components of the i th wheel along the y -axis and z -axis, respectively; f_{vby}^S and f_{vzb}^S are the forces on the vehicle body due to the deformation of the suspension system along the y -axis and z -axis, respectively; m_{vbx}^S , m_{vby}^S , and m_{vzb}^S are the moments due to the deformation of the suspension system about the x -axis, y -axis, and z -axis, respectively; f_{wiy}^S and f_{wiz}^S are the forces on the i th wheel due to the deformation of the suspension system along the y -axis and z -axis, respectively; f_{wiy}^T and f_{wiz}^T are the forces received by the i th tire from the deck are transformed from the local coordinated system of the i th wheel as

$$f_{wiy}^T = \mathbf{T}_{vwi}(2, :)(f_{wix^*}^T, f_{wiy^*}^T, f_{wiz^*}^T)^T \quad (14a)$$

$$f_{wiz}^T = \mathbf{T}_{vwi}(3, :)(f_{wix^*}^T, f_{wiy^*}^T, f_{wiz^*}^T)^T \quad (14b)$$

where $\mathbf{T}_{vwi}(j, :)$ with j ($=2, 3$) represent the vector of the j th row of the transformation matrix \mathbf{T}_{vwi} from the local coordinate system of the i th wheel (WCS) to VCS; $f_{wix^*}^T$, $f_{wiy^*}^T$, and $f_{wiz^*}^T$ are the forces received by the i th wheel from the deck along the local coordinate x^* -, y^* -, and z^* -axis of the i th wheel. In the expression of \mathbf{T}_{vwi} , steer angle δ is an input to model the behavior of a driver as

$$\delta = -\lambda_1 Y_{vb}(t - \varepsilon) - \lambda_2 v_{vbY}(t - \varepsilon) \quad (15)$$

where v_{vbY} and Y_{vb} is the velocity and the displacement from the stable lane of the vehicle body at its center on the bridge; λ_1 and λ_2 are two constants; ε is the driver reaction time. $f_{wiy^*}^T$ is approximated as zero. $f_{wiy^*}^T$ is related to the sideslip angle α and $f_{wiz^*}^T$ as

$$f_{wiy^*}^T = f(f_{wiz^*}^T, \alpha) \quad (16)$$

α is defined as

$$\alpha = \arctan \frac{v_{wiy^*}}{v_{wix^*}} \quad (17)$$

where v_{wix^*} and v_{wiy^*} are the relative velocities of the i th wheel center to the contact point on the bridge deck and can be expressed as

$$\begin{aligned} v_{wix^*} &= \mathbf{T}_{wiv}(1, :)(v_{wix} - v_{dix}, v_{wix} - v_{diy}, v_{wiz} - v_{diz})^T \\ &= \mathbf{T}_{wiv}(1, :)(v_{wix}, v_{wix}, v_{wiz})^T - \mathbf{T}_{wiv}(1, :)\mathbf{T}_{ve}(v_{dix}, v_{diy}, v_{diz})^T \end{aligned} \quad (18)$$

Similarly

$$v_{wiz^*} = \mathbf{T}_{wiv}(2,:) (v_{wix}, v_{wiy}, v_{wiz})^T - \mathbf{T}_{wiv}(2,:) \mathbf{T}_{ve} (v_{diX}, v_{diY}, v_{diZ})^T \quad (19)$$

where $\mathbf{T}_{wiv}(j,:)$ with j ($=1, 2$) represent the vector of the j th row of the transformation matrix \mathbf{T}_{wiv} from VCS to WCS of the i th wheel; \mathbf{T}_{ve} is the transformation matrix from ECS coordinate system (ECS with three orthogonal axes $X, Y,$ and $Z,$ is attached to the global system of the bridge) to VCS; $v_{diX}, v_{diY},$ and v_{diZ} are the velocity components of the contact point of the i th wheel on the deck along $X-, Y-,$ and $Z-$ axis in ECS and should be solved from the bridge subsystem.

$f_{wiz^*}^T$ is expressed as the rational function of the relative displacement and velocity along z^* between the center of the i th wheel and the corresponding contact point on the deck as

$$f_{wiz^*}^T = \begin{cases} f(Z_{wi} - Z_{pi}, Z_{wi} - \dot{Z}_{pi}) & \text{if } (Z_{wi} - Z_{pi} < h_a) \\ 0 & \text{else} \end{cases} \quad (20)$$

where h_a is the allowed displacement difference between the wheel center and the contact point on the ground and approximated as the radius of the tire without deformation. Z_{pi} and \dot{Z}_{pi} are the actual surface profiles of the bridge deck under the i th tire and should be solved from the bridge subsystem.

4.2 Bridge subsystem

The bridge subsystem is presented using the conventional Finite Element Method (FEM). Spatial beam elements of six DoFs at each end node are adopted to build the decks, towers, and piers numerically. Bar elements with three translational DoFs at each end node are used for the cables of the cable-stayed bridge. For each element, an element stiffness matrix in its local coordinate system can be generated based on the virtual work principle or other methods to describe its load resistance property. All the element stiffness matrixes are assembled eventually in the global coordinate system as \mathbf{K}_b . The mass matrix \mathbf{M}_b is formed using the lumped or consistent mass method. The structural damping matrix \mathbf{C}_b is assumed as Reyleigh damping and expressed as follows

$$\mathbf{C}_b = a_0 \mathbf{M}_b + a_1 \mathbf{K}_b \quad (21)$$

with

$$a_0 = \frac{2\omega_i \omega_j (\omega_i \xi_j - \omega_j \xi_i)}{\omega_i^2 - \omega_j^2}, \quad a_1 = \frac{2(\omega_i \xi_i - \omega_j \xi_j)}{\omega_i^2 - \omega_j^2} \quad (22)$$

where ω_i and ω_j are the frequencies of the i th and j th order modal, respectively; ξ_i and ξ_j are the damping ratios of the i th and j th order modal, respectively. The detailed process and formation of \mathbf{M}_b and \mathbf{K}_b can be found in many textbooks related to the application of the FEM to structures of linear elements, such as Xu and Xia (2012). The equations of motion of a long span bridge in FEM

in the global system are expressed as

$$\mathbf{M}_b \ddot{\boldsymbol{\delta}}_b + \mathbf{C}_b \dot{\boldsymbol{\delta}}_b + \mathbf{K}_b \boldsymbol{\delta}_b = \mathbf{F}_b^W + \mathbf{F}_b^V \quad (23)$$

where the subscript b represent the bridge; $\boldsymbol{\delta}_b$, $\dot{\boldsymbol{\delta}}_b$, and $\ddot{\boldsymbol{\delta}}_b$ are the vectors of the nodal displacement, velocity, and acceleration of all the elements; \mathbf{F}_b^W is the vector of wind loads acting on the nodes of the bridge; and \mathbf{F}_b^V is the vector of contact forces transformed from the vehicle subsystem.

4.3 Interaction of subsystems

The contact forces both in the vertical and lateral directions from the tires act on the bridge deck, causing the dynamic responses of the bridge. The displacements of the bridge deck change the moving tracks of the tires, in return.

4.3.1 Contact forces transformed from vehicle to bridge

During the movement of the vehicle, the contact force vector on the i th tire $(f_{wix}^T, f_{wiy}^T, f_{wiz}^T)^T$ counteract on the deck at the location of the tire of the magnitude $(-f_{wix}^T, -f_{wiy}^T, -f_{wiz}^T)^T$ in the WCS coordinate system. Through the following transformation, they are enforced on the bridge subsystem in the global system.

$$(F_{bwiX}^V, F_{bwiY}^V, F_{bwiZ}^V)^T = -\mathbf{T}_{ev} \mathbf{T}_{vwi} (f_{wix}^T, f_{wiy}^T, f_{wiz}^T)^T \quad (24)$$

where $(F_{bwiX}^T, F_{bwiY}^T, F_{bwiZ}^T)^T$ is the contact force vector transformed from the vehicle to the deck along the X -, Y - and Z -axes in the global system, respectively. The contact forces on all the tires can be assembled as \mathbf{F}_b^V in Eq. (23).

4.3.2 Geometric compatibility between bridge and vehicle

The geometric contact boundaries of the wheels of the moving vehicle are formed from the superposition of the displacements of the bridge deck and the road roughness. The actual surface profile Z_p under the wheels can then be expressed as follows

$$Z_p(X, Y) = Z_b(X, Y) + Z_g(X, Y) \quad (25)$$

where (X, Y) is the plane coordinate on the bridge deck with X points to the longitudinal direction and Y points to the lateral direction; Z_g is the road roughness height; Z_b is the vertical displacement of the bridge deck, and it is expressed as the function of the vertical displacement Z_{bc} and the rotational displacement θ_{Xbc} around the X -axis at the central axis of the bridge deck as

$$Z_b(X, Y) = Z_{bc}(X) + Y\theta_{Xbc}(X) \quad (26)$$

At any X , the displacements vector of the central axis of the bridge deck can be interpolated from the geometric displacements of the two end nodes of corresponding elements through the interpolation in terms of element shape functions as

$$Z_{bc}(X) = \mathbf{N}_Z^e(\xi_{eX}) \begin{Bmatrix} \delta_{bl}^{eX} \\ \delta_{br}^{eX} \end{Bmatrix}; \quad \theta_{Xbc}(X) = \mathbf{N}_{\theta X}^e(\xi_{eX}) \begin{Bmatrix} \delta_{bl}^{eX} \\ \delta_{br}^{eX} \end{Bmatrix} \quad (27)$$

where eX represents the element of the deck at the designated location X ; ξ_{eX} is the coordinate of the location X referred to the node of the element eX ; \mathbf{N}_Z^e and $\mathbf{N}_{\theta X}^e$ are the element shape functions for the vertical and rotational displacements; δ_{bl}^{eX} and δ_{br}^{eX} are the left and right end nodes of the element eX .

The time deviation of the surface profile thus becomes

$$\dot{Z}_p(X, Y) = [\dot{Z}_{bc}(X) + Y\dot{\theta}_{Xbc}(X) + \frac{\partial Z_g}{\partial X}] \dot{X} + (\theta_{Xbc}(X) + \frac{\partial Z_g}{\partial Y}) \dot{Y} \quad (28)$$

with

$$\dot{Z}_{bc}(X) = \frac{\partial \mathbf{N}_Z^e}{\partial X} \begin{Bmatrix} \delta_{bl}^{eX} \\ \delta_{br}^{eX} \end{Bmatrix} \dot{X} + \mathbf{N}_Z^e(\xi_{eX}) \begin{Bmatrix} \dot{\delta}_{bl}^{eX} \\ \dot{\delta}_{br}^{eX} \end{Bmatrix} \quad (29a)$$

$$\dot{\theta}_{Xbc}(X) = \frac{\partial \mathbf{N}_{\theta X}^e}{\partial X} \begin{Bmatrix} \delta_{bl}^{eX} \\ \delta_{br}^{eX} \end{Bmatrix} \dot{X} + \mathbf{N}_{\theta X}^e(\xi_{eX}) \begin{Bmatrix} \dot{\delta}_{bl}^{eX} \\ \dot{\delta}_{br}^{eX} \end{Bmatrix} \quad (29b)$$

The velocities of the contact point (v_{dX}, v_{dY}, v_{dZ}) at the coordinate (X, Y, Z) on the bridge deck to generate the lateral force on the wheels of the vehicle (Eq. (18)) can also be determined from the responses of the deck as follows

$$v_{dY} = \dot{Y}_{bc}(X) + d_Z \dot{\theta}_{Xbc}(X) \quad (30a)$$

$$v_{dY} = \dot{Y}_{bc}(X) + d_z \dot{\theta}_{Xbc}(X) \quad (30b)$$

$$v_{dZ} = \dot{Z}_{bc}(X) + d_Y \dot{\theta}_{Xbc}(X) \quad (30c)$$

where d_Y and d_Z represent the relative position of the contact point to the centroid of the deck section at X ; \dot{X}_{bc} and \dot{Y}_{bc} are the velocity of the centroid of the deck section along the X - and Y -axis, respectively; $\dot{\theta}_{Ybc}$ and $\dot{\theta}_{Zbc}$ are the angular velocity of the deck section around the Y - and Z -axis, respectively. Similar to \dot{Z}_{bc} and $\dot{\theta}_{Xbc}$ in Eq.29, \dot{X}_{bc} , \dot{Y}_{bc} , $\dot{\theta}_{Ybc}$, and $\dot{\theta}_{Zbc}$ can also be interpolated from the element shape function and the nodal displacement.

5. Case study

A long span highway cable-stayed bridge built in Mainland China is taken as an example. Its elevation is shown schematically in Fig. 2. It was designed with two towers and a main span of 688m. The cross section of its deck is 34.0 m wide and 3.5 m high, carrying a dual two-lane highway on its upper surface. The natural frequencies of the first mode shape of the bridge in the lateral bending, vertical bending and torsion are 0.196 Hz, 0.243 HZ, and 1.024 Hz, respectively.

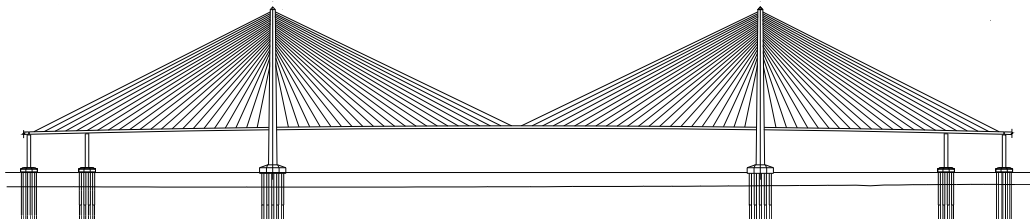


Fig. 2 Elevation of a long span cable-stayed bridge

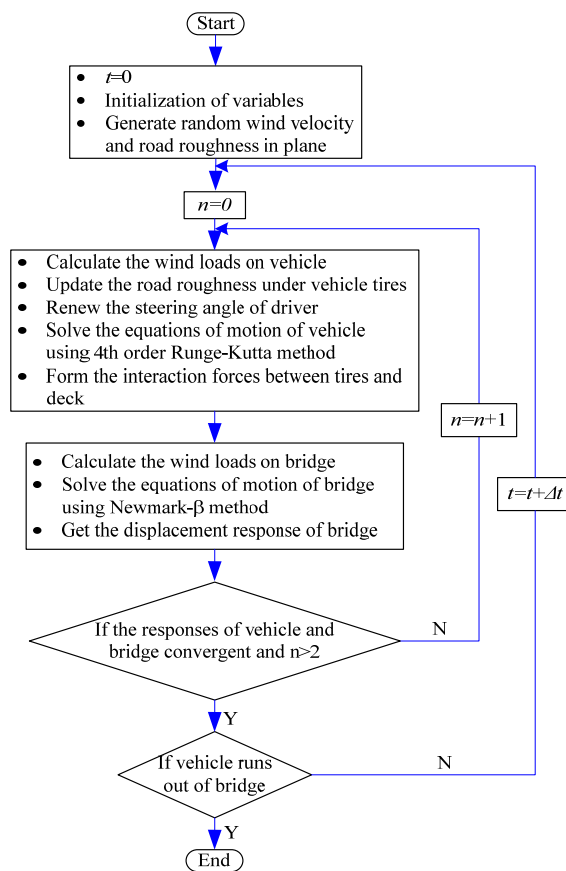


Fig. 3 Flow chart for the analysis

The damping ratio is set as 1%. The static aerodynamic coefficients C_D , C_L , and C_M of the pure deck without vehicles are shown in Xu (2013). The aerodynamic admittance functions between the buffeting forces and the fluctuating winds are assumed as units. Since the geometric section of the deck is in a streamline form with a high ratio of width to height, the flutter derivatives of the deck are approximated using those of an ideal thin plate derived by Theodorsen (1935). Bogsjö (2008) recommended an exponentially decreasing coherence model to consider the cross coherence

function of road roughness as

$$r(\Omega) = \exp(-\rho_r t_w \Omega) \tag{31}$$

where $r(\Omega)$ is the coherence coefficient for spatial frequency Ω ; ρ_r is the parameter to be determined, and t_w is the lateral distance between the two paths. After measuring 20 roads, the parameter ρ_r was founded in the range from 3.1 to 5.5. To generate a roughness plane of road surface, the exponential model is selected in this study and ρ_r is set as an moderate value of 4.0. The spectral representation method (Shinozuka 1971) is employed to generalize the surface roughness in plane with Class B and the random fluctuating wind field.

The high-sided road vehicle used in Xu and Guo (2004) is used. Generally, wind velocity on the first upwind lane is larger than that on the other lanes. The high-sided vehicle is thus located in the first lane in the upwind direction. The vehicle moves with a moderate speed of 60 km/h under the crosswind of 10m/s mean speed. To obtain stable responses, the vehicle starts at 277.8 m away from the left end of the bridge. It then moves on the bridge deck at 16.668s, reaches the middle span of the bridge at 57.947s, and finally gets out of the bridge deck at 99.227s. The constant pair (λ_1, λ_2) for the driver model in Eq. (15) is selected with the moderate value of (0.2, 0.7). The flow chart for the analysis is shown in Fig. 3. In the analysis, the time t is advanced with a time step Δt of 0.001s.

5.1 Dynamic responses of bridge

Fig. 4 shows the lateral and vertical displacements of the middle span of the bridge deck. Since the drag coefficient of the deck and the side coefficient of the moving vehicle are positive, the lateral wind forces (including the mean wind force) acting on the deck and transformed from the vehicle, and accordingly the resulted lateral displacements, are all positive. It can be seen from Fig. 4 that as the vehicle moves to the middle span (about 57.9s), the vertical displacement of the bridge deck at the middle span reaches the maximum value (the absolute value) while it reaches the minimum value when the vehicle moves at the middle positions of the two side spans. The predominant frequency of the translational displacement response in the lateral and vertical direction is consistent with the first natural frequency in the lateral bending and vertical bending, respectively. Fig. 5 shows the torsional angle of the section at the middle span of the bridge deck. As the vehicle approaches the middle span, the torsional angle reaches the maximum value (absolute value). The negative angle of the bridge deck at the middle span is due to the location of the vehicle being on the first lane of the bridge. The predominant frequency of the torsional angle is consistent with the first natural frequency of torsional vibration of the bridge. For a single vehicle passing over the bridge, all the maximum displacements of the bridge at its middle span are small.

In the previous study of the WVB system, the aerodynamic coefficients of the bridge under moving vehicles were approximated using these of the pure deck, and at the same time, the aerodynamic coefficients of the vehicle were approximated using those of the vehicle on the ground. The actual aerodynamic coefficients of both the bridge deck and the moving vehicle are studied, and therefore, the uncertainty analysis of the approximation can be investigated. Figs. 6 and 7 show the translational displacements and torsional angle of the deck at the middle span, respectively. There are only slight differences in the translational and vertical displacements for the bridge at the middle span by using the two types of aerodynamic coefficients. However, if the

actual aerodynamic coefficients of both the deck and the moving vehicle are used, the torsional angle of the bridge deck at the middle span becomes much larger and vibrates when the vehicle approaches the middle span.

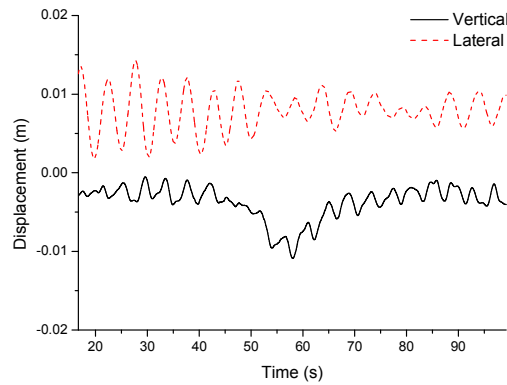


Fig. 4 Lateral and vertical displacements of the bridge in the middle span

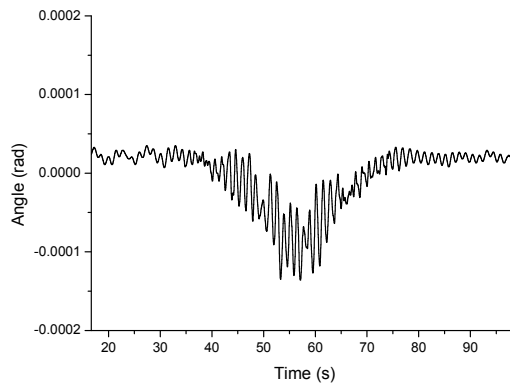


Fig. 5 Torsional angle of the bridge in the middle span

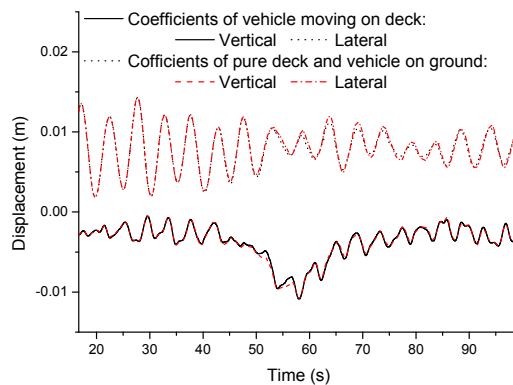


Fig. 6 Comparison of the translational displacements of the bridge in the middle span

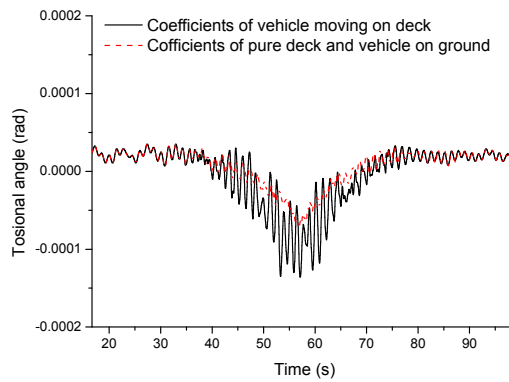


Fig. 7 Comparison of the angular displacements of the bridge in the middle span

5.2 dynamic responses of vehicle

By using the aerodynamic coefficients of the moving vehicle on the bridge deck and those of the deck with the influence of the moving vehicles, the dynamic responses of the high-sided vehicle moving on the bridge deck are calculated. Figs. 8 and 9 show the lateral displacement and yaw angle, respectively, of the vehicle body as the vehicle moves on the bridge deck. Obvious lateral and yawing motions of the vehicle can be observed for the vehicle under the combined action of crosswind, driver, and bridge motion.

Fig. 10 shows the vertical displacement of the gravity centre of the vehicle body as the vehicle moves on the bridge deck. Apart from the fluctuating components, the vertical displacement of the vehicle is consistent with the vertical displacement of the bridge deck under the vehicle. Generally, the vertical displacement of the deck reaches valleys when the vehicle moves on the middle section of each span. This can be observed in the vertical displacement of the vehicle body at about 27s, when the vehicle moves to the middle section of the left side span, at about 57.9s, when the vehicle moves to the middle section of the main span, and at about 88.9s, when the vehicle moves to the middle section of the right side span.

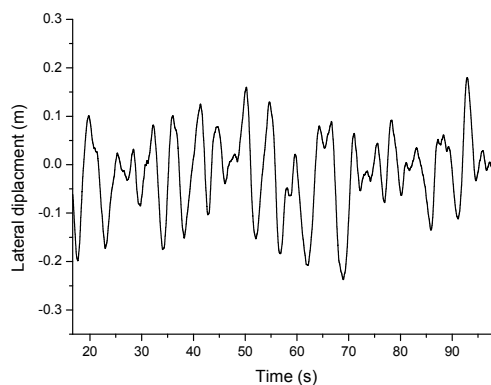


Fig. 8 Lateral displacement of the vehicle on the deck

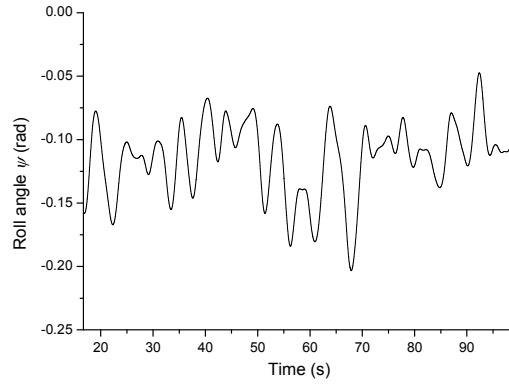


Fig. 9 Yaw angle of the vehicle on the deck

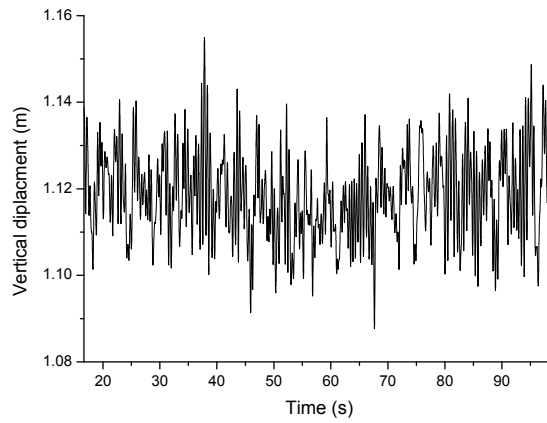


Fig. 10 Vertical displacement of the vehicle on the deck

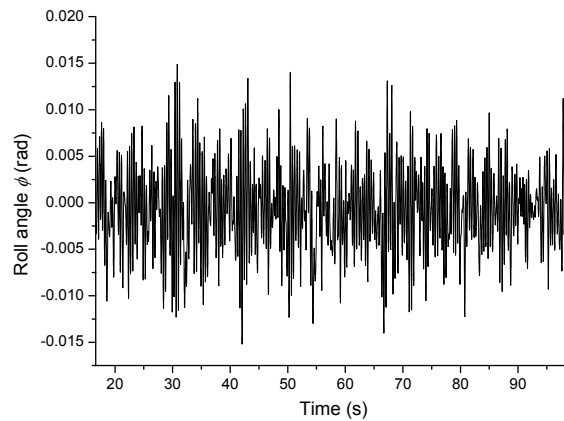


Fig. 11 Roll angle of the vehicle on the deck

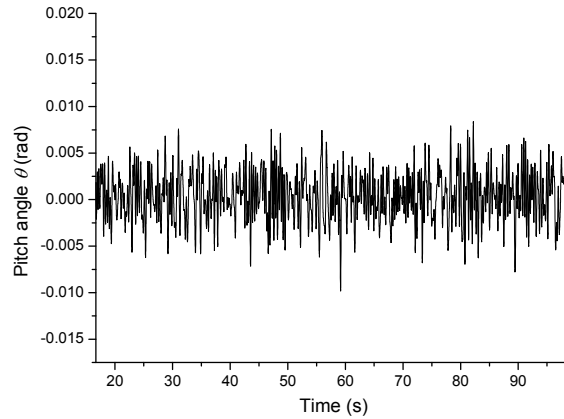


Fig. 12 Pitch angle of the vehicle on the deck

Figs. 11 and 12 show the roll and pitch angles, respectively, of the vehicle body as the vehicle moves on the bridge deck. Although their magnitudes are very small, they vary in high frequency mainly due to the road roughness and the crosswind. Figs. 13 and 14 display the acceleration responses at the seat of the driver in the lateral and vertical directions, respectively, as the vehicle moves on the deck. The fluctuating magnitude of acceleration in the lateral direction is similar to that in the vertical direction. Figs. 15 and 16 show the amplitude spectrums of the acceleration responses at the seat of the driver. Peaks occur at the natural rotating frequency and steer angle frequency in the lateral direction while peaks occur at the natural vertical frequency in the vertical direction. Moreover, small bulges can be found in the amplitude spectrum of acceleration response in the lateral direction in low frequency range, which corresponds to the natural frequency of the bridge in the lateral direction.

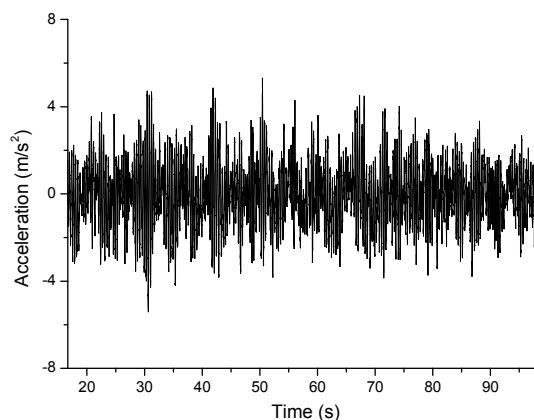


Fig. 13 Lateral acceleration at the driver's seat

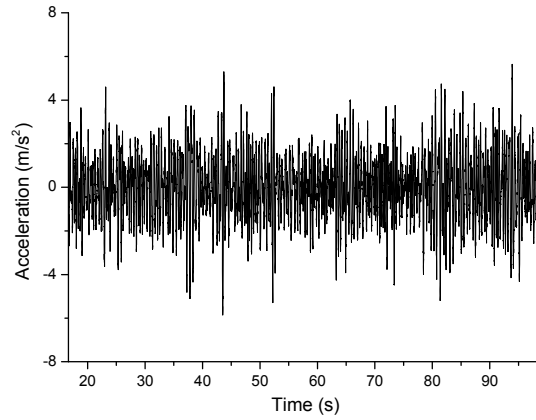


Fig. 14 Vertical acceleration at the driver's seat

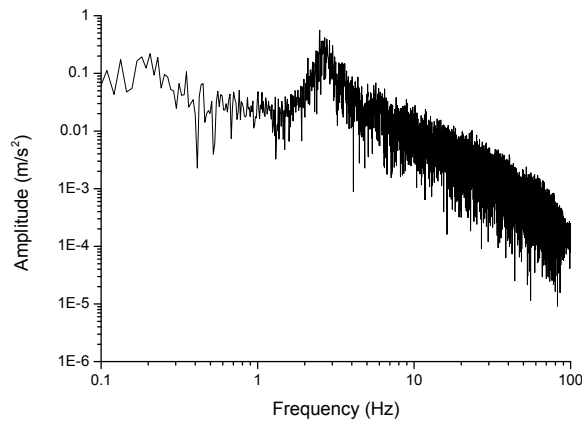


Fig. 15 Amplitude spectrum of the acceleration at the driver's seat in the lateral direction

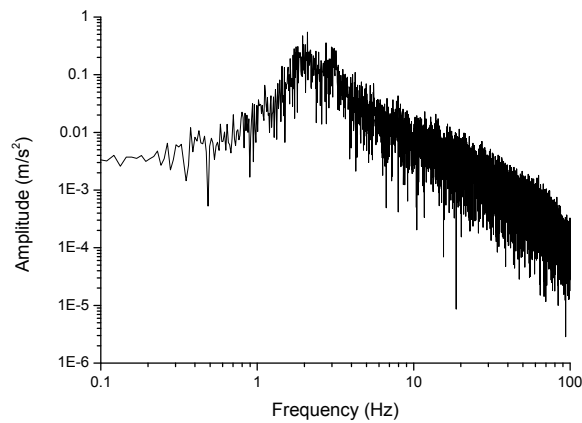


Fig. 16 Amplitude spectrum of the acceleration at the driver's seat in the vertical direction

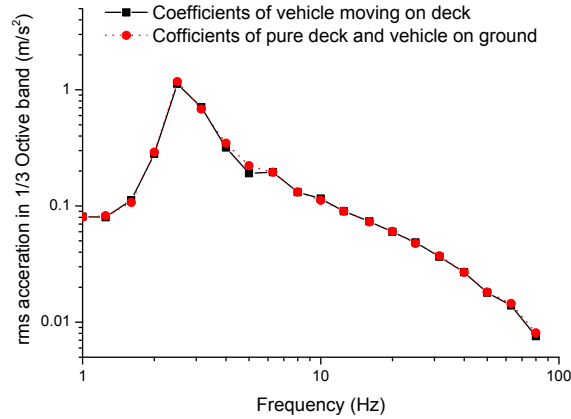


Fig. 17 rms acceleration of the vehicle at the seat in the lateral direction

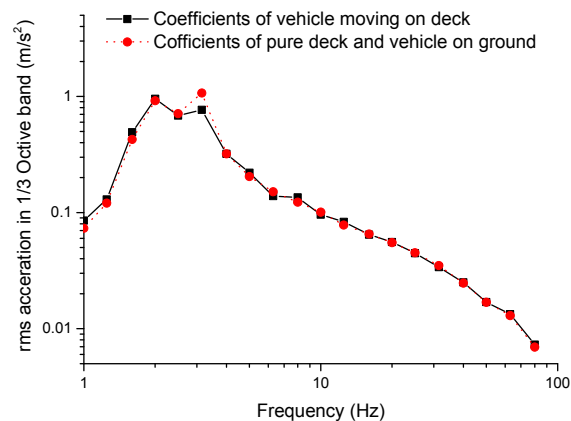


Fig. 18 rms acceleration of the vehicle at the seat in the vertical direction

Figs. 17 and 18 show the rms acceleration responses at the driver’s seat in both lateral and vertical directions on octave third band by using the two types of aerodynamic coefficients: one uses the aerodynamic coefficients of the deck under the moving vehicles and the aerodynamic coefficients of the moving vehicle with the influence of the bridge deck; the other uses the aerodynamic coefficients of the pure deck and the aerodynamic coefficients of the vehicle on the ground. It can be seen that in both lateral and vertical directions, the rms acceleration responses obtained using the actual aerodynamic coefficients of both the moving vehicle and the deck are at the same level as those using the approximate aerodynamic coefficients at a few dominant frequencies. This may be contributed to that the aerodynamic coefficient difference of the vehicle on the ground and the deck is not great and the length ratio of the vehicle to the bridge is relative small in this study.

6. Conclusions

In this study, the wind loads in WVB system updated with the computed aerodynamic parameters, considering the mutual interference between the bridge deck and the moving vehicle. And a further WVB system framework, incorporating a driver and road roughness in plane, is proposed to fully consider the lateral motion of the road vehicle on the deck under crosswind. For a single high-sided road vehicle passing by a long span bridge, the adoption of the aerodynamic coefficients of a road vehicle on the ground and the aerodynamic coefficients of the pure bridge deck for a single vehicle passing over the bridge deck may lead to an underestimation of the torsional angular response of the bridge. This will hamper the safety and ride comfort of the road vehicle. Obvious lateral and yaw motions of the vehicle occur under the combined action of wind, driver, and bridge motion. In the amplitude spectrums of the lateral acceleration responses at the driver's seat, spectral peaks occur at the natural rotational frequency of the vehicle as well as with the steer angle frequency of the driver; whereas in the vertical direction, spectral peaks occur at the natural vertical frequency of the vehicle. As the single high-sided road vehicle passes over a long span bridge in this study, the adoption of the aerodynamic coefficients of a road vehicle on the ground and the aerodynamic coefficients of the pure bridge deck for a single vehicle passing over the bridge deck may lead to the same level of the rms accelerations of the vehicle when compared to the actual aerodynamic coefficients in the situation of the moving vehicle on the deck. The studies about different types and numbers of vehicle need to be further studied in the future.

Acknowledgements

The authors wish to acknowledge the financial supports from the Research Grants Council of the Hong Kong (PolyU 5311/07E), a niche area project (PolyU 1-BB20) to the second author, research projects of Ministry of Transport of the People's Republic of China (2014319J13100, 2014318800240), and the Sichuan Province Youth Science and Technology innovation Team (2015TD0004).

References

- Bucher, C.G. and Lin, Y.K. (1988), "Stochastic stability of bridges considering coupled modes", *J. Eng. Mech. - ASCE*, **114**(12), 2055-2071.
- Bogsjö, K. (2008), "Coherence of road roughness in left and right wheel-path", *Vehicle. Syst. Dyn.*, **46**(1), 599-609.
- Cai, C.S. and Chen, S.R. (2004), "Framework of vehicle-bridge-wind dynamic analysis", *J. Wind Eng. Ind. Aerod.*, **92**, 579-607.
- Chen, S.R. and Cai, C.S. (2004), "Accident assessment of vehicles on long-span bridges in windy environments", *J. Wind Eng. Ind. Aerod.*, **92**(12), 991-1024.
- Chen, Z.W., Xu, Y.L., Li, Q. and Wu, D.J. (2011), "Dynamic stress analysis of long suspension bridges under winds, railway, and highway loadings", *J. Bridge Eng. - ASCE*, **16**(3), 383-391.
- Cheung, M.S. and Chan, B.Y.B. (2010), "Operational requirements for long-span bridges under strong wind events", *J. Bridge Eng. - ASCE*, **15**(2), 131-143.
- Han, Y., Cai, C.S., Zhang, J., Chen, S., and He, X. (2014), "Effects of aerodynamic parameters on the dynamic responses of road vehicles and bridges under cross winds", *J. Wind Eng. Ind. Aerod.*, **134**, 78-95.

- Li, Y.L., Qiang, S.Z., Liao, H.L. and Xu Y.L. (2005), "Dynamics of wind-rail vehicle-bridge systems", *J. Wind Eng. Ind. Aerod.*, **93**(6), 483-507.
- Kwon, S.D., Lee, J.S., Moon, J.W. and Kim, M.Y. (2008), "Dynamic interaction analysis of urban transit maglev vehicle and guideway suspension bridge subjected to gusty wind", *Eng. Struct.*, **30**(12), 3445-3456.
- Scanlan, R.H. (1978), "The action of flexible bridges under wind. II: Buffeting theory", *J. Sound Vib.*, **60**(2), 201-211.
- Shinozuka, M. (1971), "Simulation of multivariate and multidimensional random process", *J. Acoust. Soc. Am.*, **49**(1), 357-368.
- Wang, B. (2014), *Crosswind effects on road vehicles moving on ground and long-span bridges*, Ph.D Dissertation, The Hong Kong Polytechnic University.
- Wang, B., Xu, Y.L., Zhu, L.D., Cao, S.Y. and Li, Y.L. (2013), "Determination of aerodynamic forces on stationary/moving vehicle-bridge deck system under crosswinds using computational fluid dynamics", *Eng. Appl. Comp. Fluid Mech.*, **7**(3), 355-368.
- Xia, H., Guo, W.W., Zhang, N. and Sun G.J. (2008), "Dynamic analysis of a train-bridge system under wind action", *Comput. Struct.*, **86**(19-20), 1845-1855.
- Xu, Y.L. and Guo, W.H. (2003), "Dynamic analysis of coupled road vehicle and cable-stayed bridge systems under turbulent wind", *Eng. Struct.*, **25**(4), 473-486.
- Xu, Y.L. (2013), *Wind effects on cable-supported bridges*, John Wiley & Sons, Singapore.
- Xu, Y.L. and Guo, W.H. (2004), "Effects of bridge motion and crosswind on ride comfort of road vehicles", *J. Wind Eng. Ind. Aerod.*, **92**(7-8), 641-662.
- Xu, Y.L., Xia, H. and Yanh Q.S. (2003), "Dynamic response of suspension bridge to high wind and running train", *J. Bridge Eng. - ASCE*, **8**(1), 46-55.
- Xu, Y.L. and Xia, Y. (2012), *Structural health monitoring of long-span suspension bridges*, Taylor & Francis, UK.
- Theodosen, T. (1935), *General theory of aerodynamic instability and the mechanism of flutter*, NACA Report No. 496.